JOURNAL OF OPTOELECTRONICS AND ADVANCED MATERIALS Vol. 11, No. 3, March 2009, p. 296 - 301

Role of modified active surface sites of magnesium ferrite for humidity sensing

R. K. KOTNALA*, JYOTI SHAH, M. C. MATHPAL, DEVINDER GUPTA, L. P. PUROHIT[a], HARI KISHAN
Magnetic Materials and measurement Group, National Physical Laboratory, India
[a]*Gurukul Kangri Vishwavidyalaya Haridwar India*

Humidity response of $Mg_{1-x/2}Li_{x/4}Ce_{x/4}Fe_2O_4$ ($0.0 \le x \ge 0.4$) was studied in the range 20% - 80% RH using standard humidity generator. The LiCe substitution in magnesium ferrite decreased the grain size and pore size distribution of magnesium ferrite. The pore size distribution in the sample prepared was decreased from 40nm to 10nm and bulk porosity increased to 41% for x = 0.2 composition. Shortest adsorption humidity response time was recorded 90s for x = 0.2 compared to $MgFe_2O_4$ sample. The adsorption-desorption humidity hysteresis curves were plotted for all samples, the area enclosed in it was extremely small. Spinel structure of the ferrite compound was confirmed by XRD peaks presence and the defective structure of the spinel compound was analyzed with Raman spectra of the different samples.

(Received March 3, 2009; accepted March 19, 2009)

Keywords: Magnesium Ferrite, Defective Structure, Scanning Electron Microscopy (SEM), Humidity Sensing, Humidity Hysteresis.

1. Introduction

Magnesium ferrite is a potential candidate for humidity sensing among resistive type relative humidity sensors. The advantages of the material are long term stability, high porosity and covers wide relative humidity range. These make resistive sensors suitable for use in control and display products for industrial, commercial, and residential applications. However, seldom a few problems associated with oxide materials are long term drift, slow response time, and adsorption/desorption hysteresis. Magnesium ferrite is a oxygen deficient material at lower sintering temperature [*1*] as well as porous, that is desirable for humidity sensing. Since defective sites on the surface are highly reactive due to unsaturated bonds [*2, 3*] provide water vapors to dissociate. Researchers have been working on this material to increase its sensitivity and shortening response time by synthesizing nano-size particles [*4, 5*]. In our previous work the addition of cerium oxide in magnesium ferrite increased intergranular porosity, surface activity hence humidity sensing. It showed a better linear humidity response curve at low RH values than pure magnesium ferrite [*6*]. While lithium ion substitution in magnesium ferrite favors smaller grains and pores. This ultimately led to increase in surface area to interact more water vapors thus improved humidity sensing. Maximum sensitivity factor was observed for highest porosity sample. Li ion substitution decreased the grain size from 200nm to 110nm. The sensitivity factor increased greatly for Li-substituted magnesium ferrite [*7*]. Therefore an attempt has been made to substitute Li and Ce both together in magnesium ferrite to extract advantages for humidity sensing over a wide RH range. In present work the combined effect of cerium and lithium ion substitution has been investigated. The base resistance of magnesium ferrite is increased by LiCe substitution. The effect of such substitution at different concentration has been studied that how morphology, porosity and humidity sensing properties of magnesium ferrite changes.

2. Experimental

2.1 Material Synthesis

Analytical grade oxides of MgO, $LiCO_3$, CeO_2 and Fe_2O_3 were used to synthesize polycrystalline samples of $Mg_{1-x/2}Li_{x/4}Ce_{x/4}Fe_2O_4$, $0.0 \le x \ge 0.4$. Metal oxide powders were mixed and ground for 1hr in pastel and mortar. Fine dry mixed powder was presintered at 800 ^{O}C in a box furnace for 12 hrs in air. Presintered powders were again ground for 1hr followed by pressing into 5mm x 3mm x 2mm rectangular pellets. The rectangular pellets were sintered at 950 ^{o}C for 8 hrs in air. Electrical Ohmic contacts were made on the two parallel corner edges (3mmx2mm) of the pellets by silver paste. Silver pasted pellets were cured at 350 ^{o}C for 1hr prior to soldering of contacts. The silver contact area is negligibly small than sample area exposed to humidity in air.

2.2 Measurements

Scanning electron microscopy analysis of fractured surfaces of sintered pellets was carried out in a LEO 404 microscope. Grain size, pore size of the samples were calculated by using statistical method. X-ray diffraction of the sintered pellets was measured at room temperature within 20-70^{O}, 2θ range using a Bruker AXS configuration operating at 40kV, 40mA with Cu Kα radiation. The formation of spinel compound was confirmed by

analyzing Raman spectroscopy with Nd:YAG laser source. For measuring change in resistivity with relative humidity, conducting wires were soldered on silver contacts of rectangular pellets. A standard humidity generator (Thunder Scientific 2500 series) was utilized for carrying out the experiment in the range 20-80 %RH at 25^{O}C.
The bulk density was calculated using equation:

$$d_{\exp} = m/v \quad (1)$$

where m and v are the mass and volume of the sample.

Porosity, P, was calculated using the formula:

$$\%P = \left(1 - d_x/d_{\exp}\right)\times 100 \quad (2)$$

where dx and dexp are the X-ray density and experimental density of the samples.

3. Results and Discussion

3.1 X-Ray Diffraction

The X-ray diffraction pattern for different bulk composition samples is shown in Figure 1. The single-phase spinel peaks are present in XRD for pure magnesium ferrite [JCPDS Card No. 36-0398]. For x = 0.1, LiCe substitution with magnesium no second phase peaks have been observed. It was supposed x=0.1 amount is soluble in lattice either on magnesium site or interstitial position. For x = 0.2 composition onwards cerium oxide peaks [JCPDS Card No. 34-0394] start to appear along with spinel peaks. No peaks of lithium compound have been observed exhibiting lithium is soluble in spinel compound as lithium is not observed upto 6 mol% in XRD pattern [*8*].

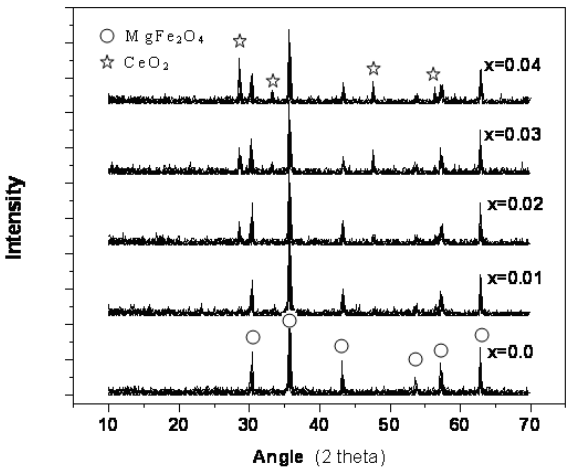

Fig 1. XRD pattern of $Mg_{1-x/2}Li_{x/4}Ce_{x/4}Fe_2O_4$ ($0.0 \leq x \geq 0.4$).

It revealed that cerium is not getting substituted into the lattice for x=0.2, only x/4 monovalent lithium ion is replacing the divalent magnesium ion in the spinel lattice. Cerium oxide peaks becomes more prominent with further increase in x value.

3.2 Raman Spectra

Raman Spectra of the composition series is shown in Figure 2. In a spinel compound with space group Oh 7 (Fd3m) five active phonon modes exist in Raman spectra [*9*]. Several small peaks along with six intense peaks have been observed at wave number 212, 291, 407, 483, 550 and 715 cm^{-1} for pure magnesium ferrite. The appearance of several small peaks exhibit defective crystal lattice field. Defective crystal field alters selection rules for intramolecular vibrations as a result some forbidden frequencies become active. When trying to substitute x=0.1 LiCe in magnesium ferrite the intensity of Raman spectra increased and thereafter decreased abruptly with x > 0.1. The intensity of the Raman spectra depends on the crystallanity of the material [*10*]. It is incorporated from XRD pattern that x=0.1 LiCe substitution diffused into the spinel lattice ultimately improving the crystallanity by compensating some defects. Beyond x = 0.1 crystallanity of the composition decreased as observed by intensity of Raman spectra and disappearance of peaks 715, 550 and 407 cm^{-1} observed since cerium was not substituted into the lattice forming CeO_2 phase. The disappearance of characteristics frequency phonon mode exhibits nonstoichiometry, vacancies, interstitial cations and defects presence in the compound, which in general may result in an activation of new phonon modes not predicted by group theory [*11*].

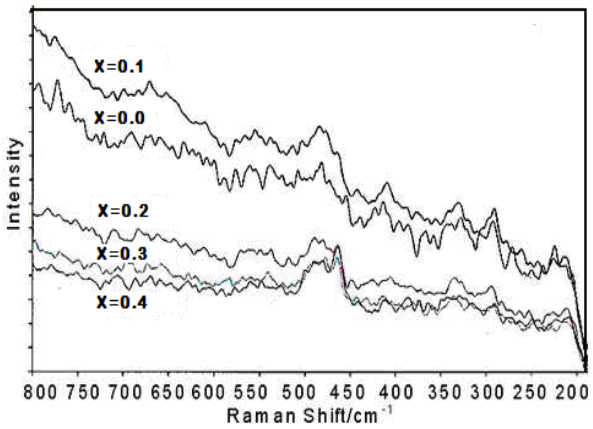

Fig 2. Raman spectra for $Mg_{1-x/2}Li_{x/4}Ce_{x/4}Fe_2O_4$ ($0.0 \leq x \geq 0.4$) using Nd:Yag laser source.

3.3 Microstructure

The surface morphology of the composition series is shown in Figure 3. The surface pore size distribution of pure magnesium ferrite is observed in the range 30nm-

50nm within mesopore range of 2nm-50nm. Small smooth compacted grains connected through grain necks are visible in SEM micrograph.

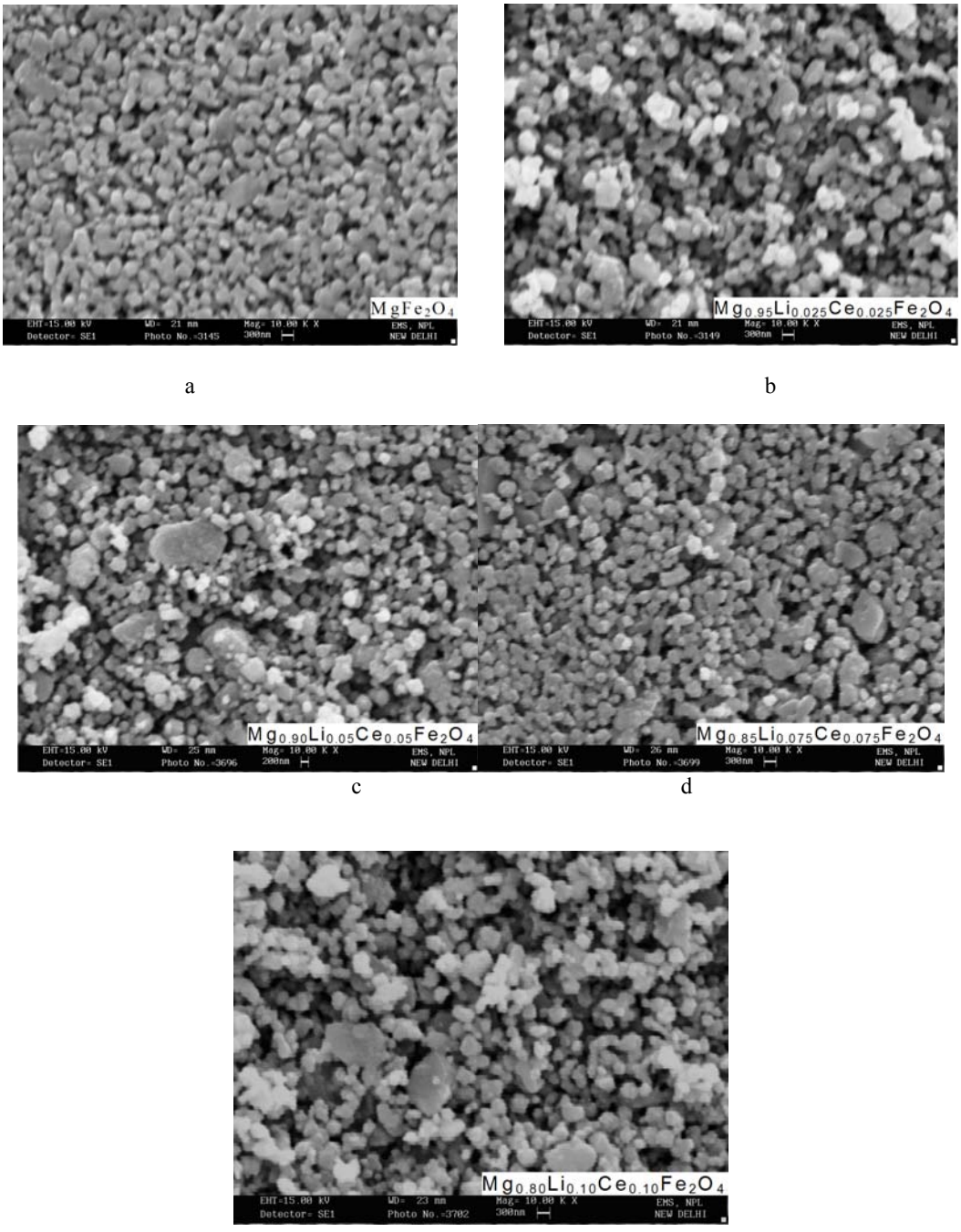

Fig 3. SEM pictures for (a) $MgFe_2O_4$, (b) $Mg_{0.95}Li_{0.025}Ce_{0.025}Fe_2O_4$, (c) $Mg_{0.90}Li_{0.05}Ce_{0.05}Fe_2O_4$, (d) $Mg_{0.85}Li_{0.075}Ce_{0.075}Fe_2O_4$, (e) $Mg_{0.80}Li_{0.10}Ce_{0.10}Fe_2O_4$.

Porosity of the bulk sample series has been given in Table 1. For x = 0.1, surface became rough and smaller grains spread over larger grains have been observed. Distribution of pore size increased in the range 40nm-1.6μm. Raman spectra intensity of the sample was maximum indicating less defective spinel compound formation hence porosity lowers. At x = 0.2 the pore size distribution measured from10nm to 40nm and grain size seems to be larger. Grains on the surface seemed smoother and highly porous. Surface of x = 0.3 composition is as

smooth as pure sample but with larger pore size distribution 10nm-500nm. Porosity of the bulk calculated decreased may be due to increasing cerium oxide concentration that segregated at grain boundary of spinel compound. Pore size distribution further increased for x = 0.4 and also grain size distribution increased.

3.4 Humidity Response

The response of resistivity to the relative humidity of Mg1-x/2Lix/4Cex/4Fe2O4 ($0.0 \leq x \geq 0.4$) series is shown in Figure 4. The RH response curve for all the compositions is linear throughout the range 20–80% RH. The spinel compound $MgFe_2O_4$ sintered at low temperature is deficient in oxygen being single phase and shows good thermal stability [*1*].

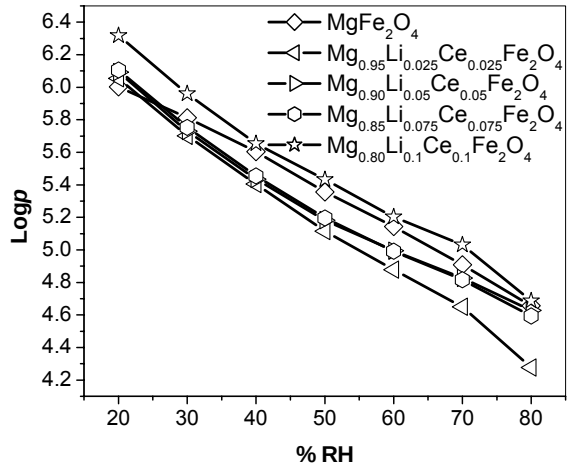

Fig 4. Logρ vs. RH curve for the sample series.

The intrinsic point defects in magnesium ferrite are oxygen vacancies i.e Schottky defects. The possible mechanism is given by

$$O_o = 1/2O_2 + 2e' + V_o^{\bullet\bullet} \quad (3)$$

For each oxygen vacancy relative to the stoichiometric oxide two Fe^{3+} are reduced to Fe^{2+}. These Fe^{2+} ions in $MgFe_2O_4$ causes porous structure [*12*]. Porosity increases resistivity of the material. It is observed that the drop in log resistivity due to increased humidity is maximum of order two for x = 0.1 composition. At this composition, either cerium has substituted magnesium ion or diffuse at interstitial position in spinel lattice. In both conditions cerium reduces Fe^{3+} ions by sucking oxygen of the lattice creating more oxygen vacancies. When oxygen deficient surface exposed to humidity dissociation of water vapor occurs and hydroxyl ion occupies the oxygen vacancies and proton binds to surface oxygen. As the humidity increases these OH^- ions provide high surface charge for water vapors and further physisorption of water vapor takes place. Conduction begins when proton hops from one water molecule to another molecule known as Groutthus chain reaction [*13*]. At high humidity condensation of water vapors starts to take place at the grain neck then into the pores. These pores acts as capillary tubes and further reduces resistivity of the material due to electrolytic conduction in addition to protonic conduction on the surface [*14, 15*]. The following substitution mechanism may take place:

$$\left[Ce_{Mg}^{\bullet\bullet}\right] = V_{Mg}'' + 2e \quad (4)$$

$$\left[Li_{Mg'}\right] = V_o^{\bullet} + h \quad (5)$$

At x = 0.1, as Ce^{4+} ion is assumed to replace Mg^{2+} ion ultimately providing free electrons to the lattice. These electrons perhaps combined with holes created by Li-substitution so no noticeable change observed in resistivity for this composition. The largest pore size distribution 1.6 μm condenses more water vapors at high RH, increasing electrolytic conduction hence resistivity drops sharply at high humidity 60% to 80% RH values. Beyond x = 0.1, CeO_2 phase is formed that segregates at grain boundary increasing the resistivity of the sample. Lithium ion replacing magnesium in spinel lattice as confirmed by the XRD analysis, no lithium compound peaks has been detected. Oxygen vacancies created by Li ions provide active surface sites for water vapors to dissociate and protons to conduct by hopping; hence resistivity decreases with increase in relative humidity.

Table 1 Experimentally calculated structural parameters and response times of composition series.

Samples	Bulk Density g/cm^3	Bulk Porosity P%	Surface Open Pores Size Distribution	Adsorption Time(s)	Desorption Time(s)
$MgFe_2O_4$	3.03	34	40nm-50nm	120	180
$Mg_{0.95}Li_{0.025}Ce_{0.025}Fe_2O_4$	3.62	23	40nm-1.6μm	120	240
$Mg_{0.90}Li_{0.05}Ce_{0.05}Fe_2O_4$	2.85	41	10nm-40nm	90	180
$Mg_{0.85}Li_{0.075}Ce_{0.075}Fe_2O_4$	2.98	39	10nm-500nm	120	180
$Mg_{0.80}Li_{0.10}Ce_{0.10}Fe_2O_4$	3.90	23	10nm-1 μm	120	180

3.5 Adsorption/Desorption Hysteresis

Desorption of water vapors from material surface always takes longer time than adsorption. This causes humidity hysteresis, hence no exactly reproducible data for RH variations is obtained. It is due to existence of non-uniformity of energy and pores [*16*]. In this series hysteresis area was found minimum associated with water vapors for the composition x=0.1 and hysteresis measured within 1% to 5% RH as shown in Figure 5. Hysteresis area increased with decreasing pore size distribution for this composition series and maximum hysteresis observed within 6% RH. To decrease hysteresis area with enlargement of pore size has been studied in detail by Björkqvist *et al* [*17*]. It suggests that due to smaller grains, water vapors get easy access to adsorb and desorb on grains which ultimately lowers the hysteresis area. The response time for the composition, series observed are within 180s as shown in Table 1.

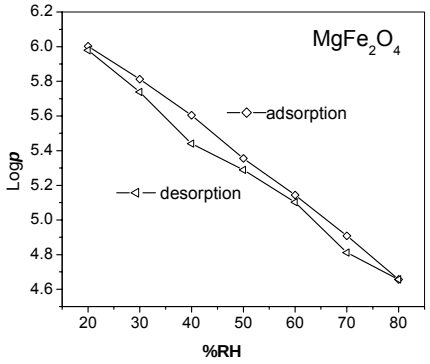

a

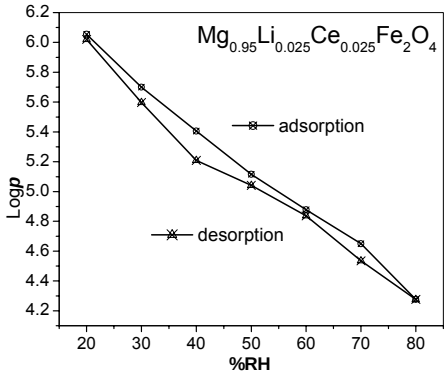

b

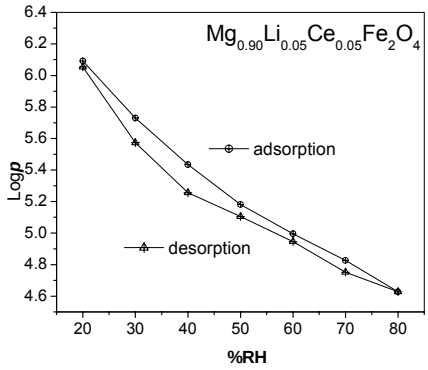

c

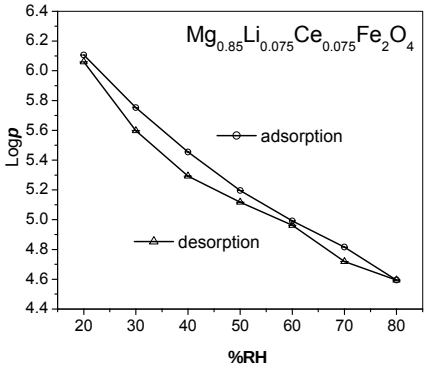

d

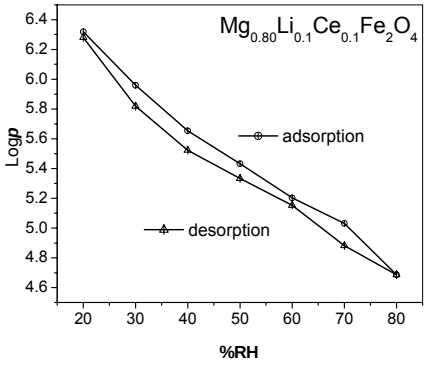

e

Fig 5. Adsorption/desorption hysteresis curve for the composition series 5(a), 5(b), 5(c), 5(d) & 5(e).

The least humidity adsorption time obtained is 90s for x = 0.2 composition sample. This composition has the smallest pore size 10nm-40nm distribution with highest porosity 41%. The smallest pore size has the highest proton conductivity due to good connectivity between water molecules [*18*].

4. Conclusions

From the results and discussion, it might be concluded that highly active surface (oxygen vacancies) and smaller pore size distribution is desirable for highly sensitive and fast humidity sensing material. High porosity with smallest open pore size distribution shorten the response time for x=0.2. The area enclosed is very small in adsorption-desorption humidity hysteresis curves of all samples prepared in this series. A low humidity hysteresis 3%-6% RH observed in this series. Moreover, combined substitution of cerium and lithium ions in magnesium ferrite is a strong potential candidate for humidity sensing by controlling grains, pores size distribution by processing conditions.

Acknowledgements

The authors are grateful to Director "National Physical Laboratory" New Delhi for providing constant encouragement, motivation and support to carry out this work. One of the authors is thankful to CSIR for granting fellowship to pursue research work.

References

[1] R. A. Candeia, M. A. F. Souza, M. I. B. Bernardi, S. C. Maestrelli, I. M. G. Santos, A. G. Souza, E. Longo, Material Res. Bulletin. **41**, 183 (2006).
[2] M. Menetrey, A. Markovits, C. Minot, Surface Sci. **524**, 49 (2003).
[3] P. Misra, R. K. Shukla, L. M. Bali, C. L.Gupta, G. C. Dubey, Sens. Actuators, B. **94**, 210 (2003).
[4] N. S. Chen, X. J. Yang, E. S. Liu, J. L. Huang, Sens. Actuators, B. **66**, 178 (2000).
[5] X. Q. Fu, C. Wang, H.C. Yu, Y. G. Wang, T. H. Wang, Nanotechnology. **18**, 145503 (2007).
[6] J. Shah, R. K. Kotnala, B. Singh, H. Kishan, Microstructure Sens. Actu. B. **128**, 306 (2007).
[7] R. K. Kotnala, J. Shah, B. Singh, H. Kishan, S. Singh, S. K. Dhawan, A. Sengupta, Sens. Actu. B. **129**, 909 (2008).
[8] G. A. El-Shobaky, N. R. E. Radwan, F. M. Radwan, Thermochimica acta. **380**, 27 (2001).
[9] Z. Wang, P. Lazor, S. K. Saxena, H. S. C. O'Neill, Mat. Res. Bull. **37**, 1589 (2002).
[10] T. F. O. Melo, S. W. da Silva, M. G. A. Soler, E. C. D. Lima, P. C. Morais Surface Science. **600**, 3642 (2006).
[11] O. N. Shebanova, P. Lazor, J. Sol. Stat. Chem. **174**, 424 (2003).
[12] J.G. Paik, Lee, M. J. Hyun, Thermochimica Acta. **425**, 131 (2005).
[13] B.M. Kulwicki, Humidity sensors. J. Am. Chem. Soc. **74**, 697 (1991).
[14] W. A. Steele, M. J. Bojan, Advc. Coll. Interface Sci. 153 (1998).
[15] B. M. Kulwicki, J. Phys. Chem. Solids. **45,** 1015 (1984).
[16] F. Detcheverry, E. Kierlik, M. L. Rosinberg, G. Tarjus, Phys. Ads. **11**, 115 (2005).
[17] M. Björkqvist, J. Paski, J. Salonen, V. P. Lehto, IEEE sensors **6**, no. 3 (2006).
[18] M. I. Tejedor, F. M. Vichi, M. A. Anderson, J. of porous materials. **12**, 201 (2005).

*Corresponding author: rkkotnala@mail.nplindia.ernet.in